Journal of Molecular Structure 1142 (2017) 18–27

Contents lists available at ScienceDirect

Journal of Molecular Structure

journal homepage: http://www.elsevier.com/locate/molstruc

FTIR, FTRaman, UV–Visible and NMR spectroscopic studies on 3,3′,4,4′-tetrachloroazoxybenzene, an azoxybenzene derivative with toxic effects

María V. Castillo [a], Jorgelina L. Pergomet [b], Gustavo A. Carnavale [b], Lilian Davies [c], Juan Zinczuk [b], Silvia Antonia Brandán [a, *]

[a] Cátedra de Química General, Instituto de Química Inorgánica, Facultad de Bioquímica, Química y Farmacia, Universidad Nacional de Tucumán, Ayacucho 471, 4000, San Miguel de Tucumán, Tucumán, Argentina
[b] Instituto de Química Rosario (CONICET-UNR), Facultad de Ciencias Bioquímicas y Farmacéuticas, Suipacha 531, 2000, Rosario, Santa Fé. R., Argentina
[c] Instituto de Investigaciones para la Industria Química (INIQUI, CONICET), Universidad Nacional de Salta, Av. Bolivia 5150, 4400, Salta, Argentina

ARTICLE INFO

Article history:
Received 3 March 2017
Received in revised form
11 April 2017
Accepted 12 April 2017
Available online 15 April 2017

Keywords:
3,3′,4,4′-Tetrachloroazoxybenzene
Vibrational spectra
Molecular structure
Force field
DFT calculations

ABSTRACT

We have synthesized 3,3′,4,4′ Tetrachloroazoxybenzene (TCAOB) and, later, characterized it by using infrared, Raman, ^{1}H, ^{13}C NMR and UV–visible spectroscopies. The structural, topological and vibrational properties of four *Cis* and three *Trans* isomers were theoretically predicted by using the hybrid B3LYP together with the 6-31G* and 6-311++G** basis sets. The 69 normal modes of vibration for all TCAOB isomers were assigned by using the scaled quantum mechanical force field (SQMFF) procedure and their experimental vibrational spectra and normal internal coordinates. The high stabilities of all *Cis* and *Trans* isomers are supported by the $\pi \rightarrow \pi^*$, $n \rightarrow \sigma^*$, $n \rightarrow \pi^*$ and $\pi^* \rightarrow \pi^*$ electronic transitions calculated by NBO studies while the AIM analyses reveal for the *Trans* forms the existence of intra-molecular C–H···O hydrogen bonds, as suggested by the broad IR band observed in the higher wavenumbers region. The low gap energy for the *Trans I* isomer supports their higher reactivity probably due to the repulsion of the more electronegative Cl and O atoms as a consequence of their proximities. In addition, the force constants for all *Cis* and *Trans* isomers were calculated by using both levels of theory. Here, the comparisons of the predicted IR, Raman, NMR and ultraviolet–visible spectra with the corresponding experimental ones demonstrate good concordances. The existence of the N=O groups in all TCAOB isomers support the differences in their properties, as compared with those reported for TCAB.

© 2017 Elsevier B.V. All rights reserved.

1. Introduction

The structural, electronic, topological and spectroscopic studies related with the 3,3′,4,4′-tetrachloroazoxybenzene (TCAOB) derivative are of great chemical and industrial interest but principally they are of interest to the human health because the presence of four Cl atoms and an azoxy group in their structure confers to it toxicological properties [1–3]. The use of these azoxybenzene derivatives as an herbicide agent produce to the people that work in contact with it, different effects such as, skin disease named chloracne, as reported by Kaufman et al. [1] and Bartha and Pramer [2]. Singh et al. have reported that in mice chronically exposed to these derivatives they developed a number of neoplastic and nonneoplastic lesions, including carcinoma of the urinary tract [3,4]. However, from an industrial point of view these derivatives have particular applications because they present photo-chemical and physical properties for which these derivatives are broadly used in multiple applications [5–15]. Structurally, these derivatives have geometrical isomers, known as *Cis* and *Trans* conformations where the mechanisms of isomerization were studied by different authors [16–18] and, where their *Trans* structures were determined for some derivatives by using X-ray diffraction [19–21]. Chemically, the irradiation photochemical of azoxybenzene by using light of wavelength less than 400 nm generate 2-hydroxyazobenzene where the photoproduct of this irradiation photochemical can be investigated by using the Raman spectroscopy, as reported by Badovinac et al. [5]. Hence, the vibrational spectroscopy is a useful tool technical to identify toxic

* Corresponding author.
E-mail address: sbrandan@fbqf.unt.edu.ar (S.A. Brandán).

http://dx.doi.org/10.1016/j.molstruc.2017.04.043
0022-2860/© 2017 Elsevier B.V. All rights reserved.

products as TCAOB and all their derivatives. Recently, the two *Cis* and *Trans* isomers of 3,3′,4,4′-tetrachloroazobenzene (TCAB) [22] have evidenced different structural and vibrational properties and, also different absorption bands. Others studies, for instance, show that the activation energy for transforming *Cis* to *Trans* forms varies with the solvent, thus, in ethanol by heating is 24.8 kcal/mol while in n-heptane the value decrease at 19.4 kcal/mol [23]. In this context, the aims of this work are to study: (i) the structural properties of TCAOB of their stable isomers and (ii) their vibrational properties in order to perform the complete assignments of their isomers because, so far, these were not reported probably as a consequence of their toxics properties. With those purposes, first, the TCAOB derivative was synthesized and then characterized it by using FTIR, FT-Raman, multidimensional NMR and UV−visible spectroscopies. Simultaneously, DFT calculations were performed in order to optimize their isomers and later, to predict their structural, electronic and topological properties by using the NBO and AIM programs [24–27]. Here, the hybrid B3LYP method was used together with the 6-31G* and 6-311++ G** basis sets [28,29]. Finally, the properties for all the TCAOB isomers were compared among them and, later, with those reported for TCAB [22] by using the same levels of theory.

2. Experimental methods

2.1. Synthesis

3,3′,4,4'-tetrachloroazoxybenzene was obtained according to protocol of Gagnon and Newbold [30] by using the following procedure.

3,3′,4,4′-Tetrachloroazobenzene (0.640 g, 0.002 mol) was dissolved in glacial acetic acid (300 ml) at 80 °C, and then 30% hydrogen peroxide (8 ml) was added. Further additions of 30% hydrogen peroxide (8 ml) were made every 15 min during the first 2 h, when a further 20 ml was added. The heating was continued at about 65 °C, then after 3 h 12 ml, and after 20 h 10 ml of 30% hydrogen peroxide was added. Heating was continued until TLC analysis showed disappearance of the starting azo compound (26 h). The solution was cooled to room temperature and poured into an excess of water (300 ml). The precipitate was filtered, dried and crystallized twice from ethanol. Yield 0.488 g (73%), m.p. = 138.5–139 °C.(Lit. 137.5–138.5 °C).

2.2. Equipments

The IR spectrum of the TCAOB solid was recorded in KBr pellets with a resolution of 1 cm^{-1}, and 64 scans between 4000 and 400 cm^{-1} on a FTIR GX1 spectrophotometer, equipped with a globar source and a DGTS (Deuterated TriGlycerine Sulfate). The Raman spectrum was recorded from 2000 to 200 cm^{-1} on a Bruker RF100/S spectrometer equipped with a Nd: YAG laser source (excitation line 1064 nm, 800 mW power) and a Ge detector at a resolution of 1 cm^{-1}, 200 scans.

Nuclear magnetic resonance (NMR) spectra were recorded on a Bruker 300 AVANCE spectrometer at 300 MHz for ^{1}H and 75 MHz for ^{13}C in $CDCl_3$ solutions containing 0.03 vol % TMS as internal standard. GC-MS spectrum was recorded on a 5973 Hewlett-Packard selective mass detector coupled to a Hewlett Packard 6890 gas chromatograph equipped with a Perkin-Elmer Elite-5MS capillary column (5% phenyl methyl siloxane, length = 30 m, inner diameter = 0.25 mm, film thickness = 0.25 μm); ionization energy, 70 eV; carrier gas: Helium at 1.0 ml/min. UV spectra were collected on a UV−Visible 160 A Shimadzu spectrophotometer.

3. Computational details

First, the initial *Cis* and *Trans* structures of TCAOB were modelled with the *GaussView* program [31] and, later, both species were optimized by using the B3LYP/6-31G* and 6-311++G** methods with the Gaussian09 program [32]. With these optimized structures the potential energy surface (PES) curves associated with the rotation around the C1−N12 bond, described by the C2−C1−N12−N13 dihedral angles and with the rotation around the N13−C14 bond, described by the N12−N13−C14−C15 dihedral angles were studied for those levels of theory. The PES for the *Cis* and *Trans* forms of TCAOB are observed in Fig. S1 and S2 using B3LYP/6-31G* level of theory (Supporting Material). For the *Cis* form, the DFT calculations show the presence of four stable conformers with geometries C_1, named *Cis-I, Cis-II, Cis-III* and *Cis IV*. For the *Trans* form Fig. S2 shows two conformers named *Trans-I* and *Trans II* by using the C2−C1−N12−N13 dihedral angle while a third stable conformer called *Trans III* is obtained by using the N12−N13−C14−C15 dihedral angle. All the *Cis* and *Trans* structures of TCAOB and the atoms numbering can be seen in Figs. 1 and 2, respectively. The natural atomic population (NPA) charges and the bond orders for the all structures were calculated with the NBO 3.1 [25] program while the topological analyses were performed by using the AIM2000 program [27]. The Merz-Kollman (MK) charges were also studied in order to calculate the molecular electrostatic potentials [33]. Here, the force fields were computed with the SQMFF procedure using both levels of theory and scale factors valid for the 6-31G* basis set [34]. The natural internal coordinates for the *Cis* and *Trans* forms of TCAOB were similar to those reported for TCAB [22]. Then, the force fields in cartesian coordinates were changed to "natural" internal coordinates with the MOLVIB program [35]. The complete vibrational assignments were performed considering energy distributions (PED) $\geq$ 9% with the SQMFF procedure [34]. The Gauge-Independent Atomic Orbital (GIAO) method [36] at B3LYP/6-31G* level of theory was used to predict the ^{1}H and ^{13}C chemical shifts of all the species using Trimethylsilane (TMS) as reference. The Time-dependent DFT calculations (TD-DFT) at the B3LYP/6-31G* level of theory was employed to predict the UV−visible spectrum of TCAOB in ethanol solution by using the Gaussian 09 program [32]. On the other hand, the energies of the frontier orbitals were used to calculate the gap energy values and some interesting descriptors in order to predict their reactivities and behaviors at the same level of theory [37–40]. The properties were analyzed for all the forms and then they were compared with those reported for TCAB [22].

4. Results and discussion

4.1. Geometry

The total energies and relative, the dipole moment values and populations for all isomers of TCAOB calculated with the B3LYP method at different levels of theory can be seen in Table 1. The calculations with both basis sets predict the energies of the three *Trans* forms significantly higher than the corresponding to the *Cis* forms, as reported by Chen and Chieh for azobenzene and stilbene [41]. Also, it is observed that the differences energies between *Trans* forms by using 6-31G* basis set are between 0.26 and 0.21 kJ/mol in gas phase and increase in solution to values between 0.31 and 0.21 kJ/mol, by using the same basis set. The difference energies of the *Cis* isomers in relation to the *Trans* ones in both media are very high, although slightly decreases in solution and, for these reasons, their populations are practically zero. Despite the low populations for the *Cis* forms they were also

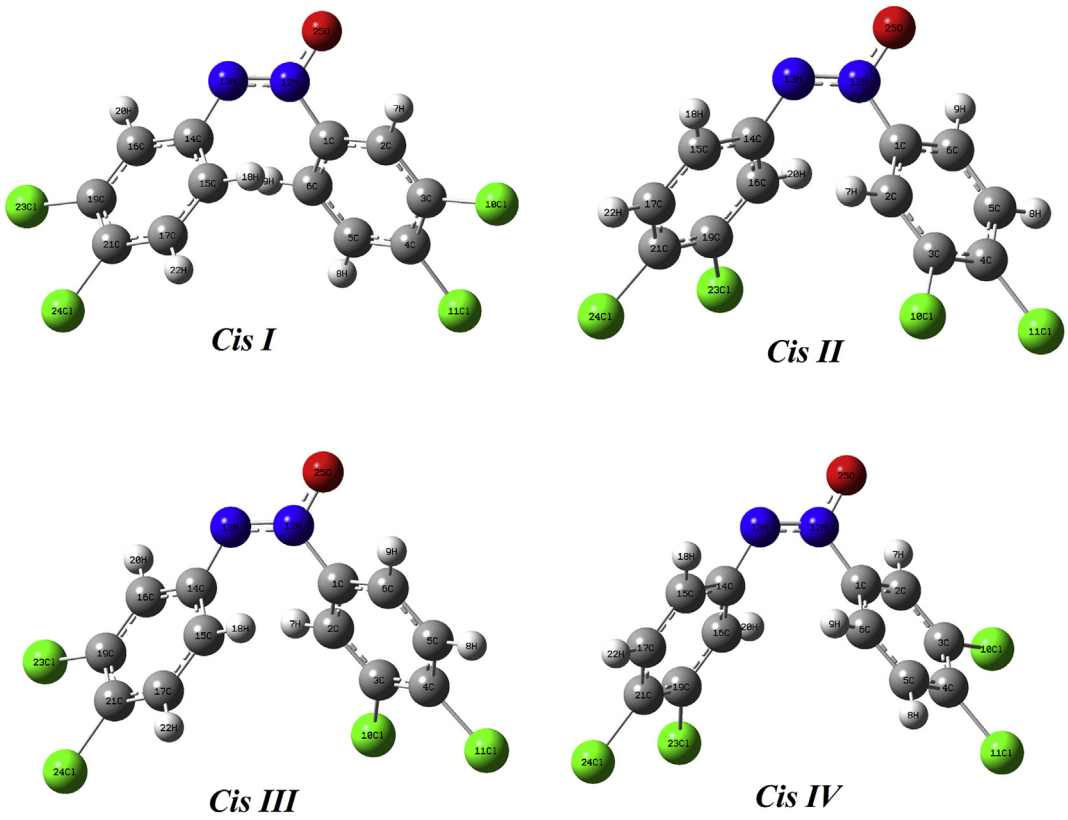

Fig. 1. Molecular structures of *Cis* isomers of TCAOB and atoms numbering.

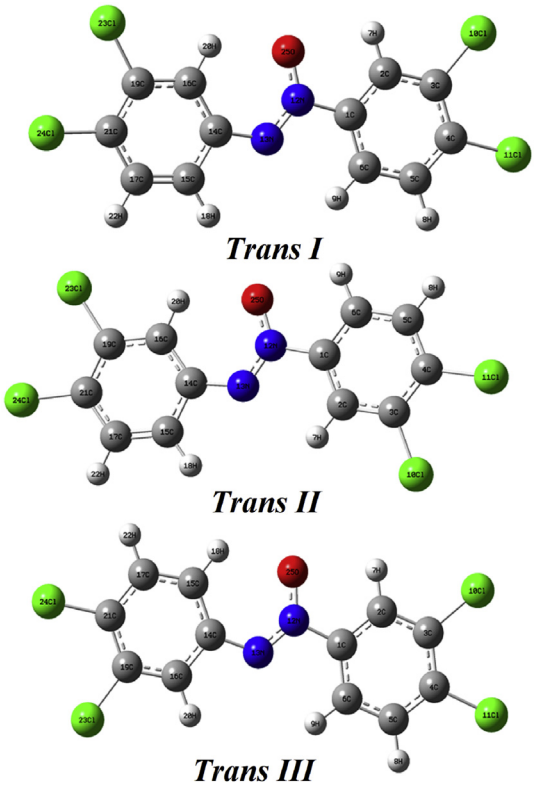

Fig. 2. Molecular structures of *Trans* isomers of TCAOB and atoms numbering.

considered in this study because it is known the existence of isomerization process among them, as reported by different authors for these derivatives [16–18] and by us for TCAB [22]. Comparing the energy values of all isomers, we observed that the *Trans-II* isomer has the lowest value which is consistent with the study of the *trans*-1,2-bis (3-chlorophenyl) diazene oxide form [21], whose structure is similar to the *Trans II* isomer of TCAOB. In that work the authors have reported that the molecule adopts a thermodynamically stable configuration in which the two groups are oriented in position *Trans* chlorophenyl with respect to the N=N bond. Table S1 and S2 shows a comparison of the calculated geometrical parameters for the *Cis* and *Trans* conformations of TCAOB by using both basis sets with the experimental values reported for *cis*-azobenzene [42], azobenzene [43], 3-(4-Chlorophenyl)quinazolin-4(3H)-one [44], *trans*-Diphenyldiazene oxide [20] and *trans*-1,2-bis(3-chlorophenyl) diazene oxide [21] by means of root mean square deviation (rmsd) values. The better rmsd values for bond lengths and angles values are obtained when these parameters are compared with the azobenzene compound, as expected because it is a similar compound. Note that the bond N12–C1–C2 and N12–C1–C6 angles and the dihedral N13–N12–C1–C2 and N13–N12–C1–C6 angles have different values in both *Cis* conformers. For the *Trans* conformations a better correlation in the bond angles is observed when their values are compared with the parameters reported by Martínez and Bernès [20] in an experimental study for *trans*-Diphenyldiazene oxide than the experimental parameters obtained to *trans*-1,2-bis (3-chlorophenyl) diazene oxide [21]. This observation could be related to that in the chlorinated compound, the authors consider that the oxygen atom is disordered over two inversion-related positions N12–O25 and N13–O25. For TCAOB, the bond lengths

Table 1
Calculated total energy (E) and relative (ΔE), dipolar moments (μ) and populations for all TCAOB isomers.

Isomers	B3LYP method							
	6-31G*				6-311++G**			
	E (Hartrees)	μ (D)	ΔE (kJ/mol)	Population Analysis(%)	E (Hartrees)	μ (D)	ΔE (kJ/mol)	Population Analysis(%)
Cis I	−2486.2904	2.42	64.3	0	−2486.5699	2.69	57.9	0
Cis II	−2486.2903	1.14	64.5	0	−2486.5701	1.38	57.6	0
Cis III	−2486.2902	3.15	64.8	0	−2486.5699	3.21	58.2	0
Cis IV	−2486.29041	2.61	64.3	0	−2486.5701	2.76	57.7	0
Trans I	−2486.3148	3.53	0.26	31.9	−2486.5919	3.53	0.31	32.9
Trans II	−2486.3149	1.88	0.0	35.5	−2486.5920	1.83	0.0	35.7
Trans III	−2486.3148	1.26	0.21	32.6	−2486.5920	1.26	0.21	31.4

N12—N13 have the intermediate values between single and double bond. Besides, in the chlorinated compound the C1—C2 and C1—C6 distances and C1—N12—N13 and N12—N13—C14 angles are similar, hence, it is possible to consider that the O atom can be in either of the two N atoms.

4.2. Molecular electrostatic potentials, atomic charges and bond orders

Due to the interesting photo-chemical and physical properties expected for TCAOB the studies of their stabilities are of great aid to analyze the isomerization process [5–15]. Thus, the stabilities and electrostatic interactions of all the isomers of TCAOB were studied through the NPA and MK charges and molecular electrostatic potentials (MEP). The results are presented from Table S3 to S5, respectively. Here, the higher molecular potentials are observed on the Cl, N and O atoms of TCAOB conformers and the values are approximately the same in all the *Cis* and *Trans* conformers, as can be seen in Table S3. The detailed analysis of all the charges shows that in general the NPA charge on N12 atom do not change to both conformational forms. On the contrary, the NPA charges on N13 atom for the *Cis* forms are slightly lower than those corresponding to the *Trans* forms of TCAOB, as shown in Fig. S3, hence, this figure shows clearly the variations of the calculated MK and NPA charges on the N12 and N13 atoms corresponding to all isomers of TCAOB at B3LYP/6-31G* level. We can see that the MK charges on N12 and N13 atoms inversely vary between the two groups of isomers. On the one hand, MK charges on the N12 atoms are higher for *Cis* isomers than for the *Trans* forms, while for the N13 atoms are higher for the *Trans* forms.

The bond order values expressed as Wiberg indexes for all isomers can be seen in Table S6 while in Table S7 and Fig. S4 show the variations of these values only for the C—N, N═N, N═O, and C—Cl bonds corresponding to the seven isomers in gas phase. Here, the higher values are observed in the N12═N13 bonds corresponding to both isomers but the *Cis* isomers present the higher values than the *Trans* ones. A similar tendency are observed in the BO values corresponding to the N12═O25 bonds. On the other hand, we observed that in the C14—N13 and C1—N12 bonds the corresponding BO values are higher in the *Trans* isomers than the *Cis* ones. In relation to the BO values corresponding to the C—Cl bonds, we observed different behaviors in both isomers, thus, for instance, the higher values for all isomers are observed on the C4—Cl11 bonds while the lower values in the C19—Cl23 bonds. A very important observation is the different BO values that present the C21—Cl24 bonds in all isomers, where the higher values are observed in the *Trans* forms probably because the position of these bonds are near to the N═O bonds in these isomers which are different from the *Cis* ones, as observed in Figs. 1 and 2. Hence, these differences among the isomers could be probably attributed to a result of resonance occurring within the molecule.

4.3. NBO and AIM studies

The stabilities of all TCAOB isomers and their topological properties were studied by using NBO [25] and AIM [27] calculations in order to investigate the existence of different donor—acceptor and intra-molecular interactions in these isomers. Those studies are of importance taking into account the photochemical properties that present these derivatives when they are used in the industry as light-triggered switches [5,6,9]. Table S8 shows the second order perturbation energies $E^{(2)}$ (donor→acceptor) corresponding to the most important delocalizations for all TCAOB isomers. Four contributions of the stabilization energies are observed in all isomers, by using both basis sets, they are: $\Delta ET_{\pi\rightarrow\pi^*}$, $\Delta ET_{n\rightarrow\sigma^*}$, $\Delta ET_{n\rightarrow\pi^*}$ and $\Delta ET_{\pi^*\rightarrow\pi^*}$ of which the first three contributions favors to the *Cis* forms while the latter to the *Cis II*, *Trans II* and *Trans III* forms. Fig. S5 shows a description graphic of these delocalizations. Note that the all *Cis* forms have the only two $\pi N12\text{-}N13\rightarrow nO25$ and $\sigma N12\text{-}O25\rightarrow nO25$ delocalizations that are not present in the *Trans* forms. Moreover, the transitions $\Delta ET_{\pi^*\rightarrow\pi^*}$ have the higher values in all *Cis* and *Trans* isomers and, for this reason, the total contribution shows that same tendency, as observed in Fig. S5.

The topological properties [26] are useful parameters to study the intra-molecular interactions of all TCAOB isomers by using the AIM2000 program [27]. In general, the exhaustive analysis shows a somewhat dependence of the topological properties with the size of the basis set when increase at 6-311++G**. Here, the analysis of the topological properties in the bond critical points (BCPs) and ring critical points (RCPs) for all isomers in gas phase by using both basis sets are presented from Table S9 to S11. Accordingly, the results show for the *Cis* isomer with both basis sets two ring critical points, RCP_1 and RCP_2 while for the *Trans* forms a third ring critical point RCP_3 it is observed, as shown in Table S9. Now, we can identify the ring bonded to the oxidized nitrogen atom as RCP_1 while the ring bonded to another nitrogen atom is RCP_2. RCP3 observed only in the *Trans* isomers are related to H bonds formed, as clearly is observed in Table S10 with both basis sets. Note that the nature of these H bonds are different in the three *Trans* isomers, thus, in *Trans I* and *II* are formed the C16—H20···O25 bonds while in the *Trans II* isomers the C15—H18···O25 bonds. Note that the topological properties of these H bonds change when the size of the basis set increase from 6-31G* to 6-311++G**. Fig. S6 shows the variations of the calculated density, Laplacian and $\lambda 1/\lambda 3$ ratio values corresponding to RCP_1 and RCP_2. The figure shows clearly that the higher (ρ) values are calculated by using 6-31G* basis set on both rings of the *Trans I* form. Therefore, the C16—H20···O25 interaction and RCP_3 are only observed in these *Trans* isomers. These AIM results are in complete agreement with the experimental resulted observed by Kavitha et al. [21] by X-ray diffraction in the crystal packing of *trans*-1,2-bis (3-chlorophenyl) diazene oxide, where the molecules are linked by intra and inter-molecular C—H···O hydrogen bonds.

4.4. Vibrational analysis

The population analyses suggest that only the *Trans* isomers of TCAOB can be present in the solid phase of this compound, as indicated in Table 1, but taking into account that the isomerization process between both isomers was experimentally reported [16–18,22], in this study, all the *Cis* isomers were also considered. These TCAOB isomers have 69 normal vibration modes showing all activity in both IR and Raman spectra. The assignments of the experimental bands to the expected normal vibration modes were made on the potential energy distribution contributions (PED) $\geq$ 9%, by using the symmetry coordinates and, taking into account the assignments for TCAB [22] and the calculation's results. The observed and calculated wavenumbers and assignments for all TCAOB isomers in gas phase by using SQM/B3LYP/6-31G* calculations are presented in Table 2. The comparisons of the experimental infrared and Raman spectra for TCAOB, by using B3LYP/6-31G* theory level, with the corresponding average predicted demonstrate good correlations as observed respectively in Figs. 3 and 4. The broad IR band centred in approximately 3440 cm^{-1} is easily assigned to the inter-molecular C–H···O hydrogen bonds, as was observed by X-ray diffraction in the crystal packing of *trans*-1,2-bis (3-chlorophenyl) diazene oxide [21] and, as reported by us for TCAB [22]. Therefore, the group of the IR and Raman bands between 3200 and 2851 cm^{-1} are justified by both *Cis* and *Trans* forms, as can be seen in both average spectra for the isomers series. The strong bands between 1500 and 1000 cm^{-1} in the experimental IR spectrum can be easily attributed to the presence of the *Trans* forms while probably in this region these bands overlap those bands associated to the *Cis* forms. On the other hand, the comparisons between the experimental IR spectra for TCAB [22] and TCAOB in the 4000/2800 and 2000/350 cm^{-1} regions (Figs. S7 and S8) show clearly the differences attributed to the N=O group in TCAOB. Thus, in the region of higher wavenumbers we observed un increase in the band centred in 3440 cm^{-1} probably because the presence of the N=O group generate higher numbers of H bonds in TCAOB. Also, a shifting of the bands assigned to the CH stretching modes is observed in this region. In the 2000/350 cm^{-1} region we observed a notable increase in the intensities of some bands observed between 1800/1500 and 1400/600 cm^{-1} while other bands decrease their intensities, as those located between 1300 and 900 cm^{-1}. Below, brief discussions of some bands are presented.

4.4.1. Assignments

4.4.1.1. C–H modes. The CH stretching modes belong to the two rings for all isomers of TCAOB can be easily assigned to the IR and Raman bands observed in the 3200/3000 cm^{-1} region while the corresponding in-plane deformation modes are associated to the IR and Raman bands between 1462 and 1097 cm^{-1}. The IR and Raman bands between 978 and 817 cm^{-1} are attributed to the out-of-plane deformation modes because in TCAB these modes were assigned between 935 and 817 cm^{-1}.

4.4.1.2. CCl modes. In TCAB, the C–Cl stretching modes were assigned between 606 and 442 cm^{-1} [22]. Here, for the *Trans* isomers these modes are clearly assigned between 795 and 372 cm^{-1} while for the *Cis* forms they are assigned between 782 and 401 cm^{-1}. SQM calculations predicted some C–Cl in-plane deformation modes at higher wavenumbers than the corresponding out-of-plane deformation modes, hence, in all isomers they were assigned as predicted by calculations and, as indicated in Table 2.

4.4.1.3. Skeletal modes. The N=N stretching modes for the *Cis* forms of TCAB were predicted by calculations at higher wavenumbers than the corresponding *trans* forms [22]. In all TCAOB isomers these modes are predicted in the same region and coupled in some isomers with other stretching modes, hence, they are assigned to the very strong IR and Raman bands at 1462 and 1478 cm^{-1}, respectively. In both TCAB isomers the N–C stretching modes were assigned in the 1209/1120 cm^{-1} region, here, these modes are assigned to the IR and Raman bands between 1202 and 1070 cm^{-1}. The rings C–C stretching modes in the TCAB isomers were assigned at 1577 and 1558 cm^{-1} and, for these reasons, these modes for all TCAOB isomers are assigned between 1577 and 1541 cm^{-1}. The remaining C–C stretching modes and the deformations and torsions of both rings are assigned as predicted by SQM calculations and, as observed in compounds with similar rings [22,38,39].

4.5. Force field

The forces constants for all TCAOB isomers were calculated employing the SQM methodology [34] and the Molvib program [35]. Their values are presented in Table 3 compared with those reported for TCAB [22]. We observed that the forces constants are slightly dependent of the size of the basis set, thus, their values decrease when increase the basis set of 6-31G* at 6-311++G**, a result also observed in TACB [22]. Analyzing the *f*(*N=N*) force constants, we observed that for the *trans* forms of TCAOB the values are higher than for the C*is* forms by using the 6-31G* basis set but a contrary result is observed with the other basis set. In TCAB, on the contrary, with both basis sets the force constants are higher for the *Cis* forms than the other ones. Besides, in TCAB the values of these constants are higher than the TCAOB. Evidently, the presences of the N=O bonds in TCAOB could in part justify these differences. Hence, for this same reason, in TCAOB the *f*(*νC-N*) force constant values for the *Trans* isomers are higher than those observed for the *Cis* isomers. On the contrary, the *f*(C–Cl) force constants for the *Cis* isomers are higher than those corresponding to the *Trans* isomers. In TCAOB, other possible explanation of the lower values observed in the *f*(*N=N*) and $f(C-C)_{ring}$ force constants for the *trans* forms could be probably related to the strong $\pi \rightarrow \pi$ delocalizations observed by NBO analysis due to the planarity of those two forms, as also was observed in the *trans* forms of TCAB [22].

4.6. NMR study

The predicted ^{1}H and ^{13}C NMR chemical shifts for all TCAOB isomers calculated by using the GIAO method [36] and the 6-31G* basis set are summarized in Table S12 and S13, respectively, compared with the corresponding experimental ones by means of the RMSD values. Here, the results for the H nucleus show a better concordance than the corresponding to the C nucleus, because their rmsd values are between 0.69 and 0.28 ppm, having the closer values the *Trans I* and *II* isomers. For the ^{13}C nucleus, the rmsd differences increase up to a 3.34–3.20 ppm range where the *Cis II* form present the better correlation and all *Trans* forms the higher values. Here, the differences could be explained in part by the B3LYP/6-31G*calculations and, on the other side, to the calculations performed in gas phase instead solution. The higher rmsd values for the C nucleus corresponding to the *Trans* forms could be attributed to the formation of H bonds where the C atoms are involved, as observed in Table S11 by AIM analysis. In general this study show that the experimental and calculated chemical shifts for both ^{1}H and ^{13}C atoms are in reasonable concordance despite the theoretical values were calculated in gas phase by using 6-31G* basis set.

4.7. HOMO–LUMO energy gap

Taking into account the toxics properties that present these

Table 2
Observed and calculated wavenumbers (cm^{-1}) and assignment for all TCAOB isomers.

Experimental[a]		*Cis I*[a]		*Cis II*[a]		*Cis III*[a]		*Cis IV*[a]		*Trans I*[a]		*Trans II*[a]		*Trans III*[a]	
IR Solid	Raman	SQM[b]	Assig.[a]	SQM[b]	Assig.[a]	SQM[b]	Assig.[a]	SQM[b]	Assig.[a]	SQM[b]	Assig.[a]	SQM[b]	Assig.[a]	SQM[b]	Assig.[a]
3135vw		3117	νC6-H9	3116	νC6-H9	3115	νC6-H9	3115	νC6-H9	3174	νC16-H20	3173	νC16-H20	3172	νC15-H18
3103w	3104vw	3112	νC2-H7	3113	νC2-H7	3112	νC2-H7	3111	νC2-H7	3134	νC2-H7	3138	νC2-H7	3133	νC6-H9
3072w	3072w	3101	νC16-H20	3101	νC16-H20	3101	νC16-H20	3101	νC16-H20	3134	νC6-H9	3130	νC6-H9	3133	νC2-H7
3051vw		3097	νC17-H22	3098	νC17-H22	3097	νC17-H22	3098	νC17-H22	3100	νC17-H22	3101	νC17-H22	3106	νC16-H20
3035w		3096	νC5-H8	3097	νC5-H8	3084	νC5-H8	3096	νC5-H8	3097	νC5-H8	3096	νC5-H8	3095	νC5-H8
3015w		3084	νC15-H18	3085	ν C15−H18	3096	νC15-H18	3085	νC15-H18	3087	νC15-H18	3088	νC15-H18	3091	νC17-H22
1577w		1585	νC15-C17	1583	νC1-C2	1584	νC1-C2	1584	νC15-C17	1589	νC1-C2	1588	νC1-C2	1588	νC1-C2
1577w		1579	νC1-C2	1578	νC15-C17	1579	νC15-C17	1579	νC1-C2	1578	νC15-C17	1579	νC15-C17	1578	νC15-C17
1561vw	1574s	1568	νC6-C1	1571	νC6-C1	1571	νC6-C1	1569	νC6-C1	1575	νC5-C6	1574	νC6-C1	1574	νC5-C6
											νC6-C1		νC5-C6		νC6-C1
1542vw	1549w	1543	νC14-C15	1546	νC14-C15	1544	νC14-C15	1546	νC14-C15						
1536vw	1540m									1537	νC17-C21	1537	νC17-C21	1531	νC17-C21
1462vs	1478s	1493	νN12═N13	1493	νN12═N13	1492	νN12═N13	1493	νN12═N13	1495	νN12═N13	1496	νN12═N13	1493	νN12═N13
1462vs	1470s	1461	β(C17−H22)	1462	β(C17−H22)	1462	β(C17−H22)	1462	β(C17−H22)	1457	β(C2−H7)	1456	β(C2−H7)	1457	β(C17−H22)
1448s	1448w	1455	β(C5−H8)	1456	β(C5−H8)	1456	β(C5−H8)	1456	β(C5−H8)	1452	νC21-C19	1451	νC21-C19	1455	νC19-C16
1380s	1382s	1388	νC19-C16	1382	νC19-C16	1388	νC19-C16	1382	νC2-C3	1383	νC19-C16	1383	νC19-C16	1384	νC19-C16
	1359w	1382	νC2-C3	1380	νC2-C3	1380	νC2-C3	1380	νC19-C16	1378	νC2-C3	1377	νC2-C3	1376	νC2-C3
1317sh	1318s	1335	νO25-N12	1341	νO25-N12	1334	νO25-N12	1341	νO25-N12						
1306s	1306vs									1313	νO25-N12	1312	νO25-N12	1321	νO25-N12
1288m	1290m	1283	νC3-C4	1283	νC3-C4	1282	νC3-C4	1284	νC3-C4	1290	νC3-C4	1291	νC3-C4	1290	νC3-C4
1270vw	1270s	1267	νC21-C19	1268	νC21-C19	1268	νC21-C19	1268	νC21-C19	1268	νC16-C14	1269	νC16-C14	1267	νN12═N13
			νN12═N13		νN12═N13		νN12═N13		νN12═N13						
1252vw	1253m	1253	β(C16−H20)	1254	β(C16−H20)	1254	β(C16−H20)	1253	β(C16−H20)	1255	β(C17−H22)	1257	β(C17−H22)	1252	β(C16−H20)
	1245m	1247	β(C2−H7)	1251	β(C2−H7)	1251	β(C2−H7)	1247	β(C2−H7)	1243	β(C5−H8)	1245	β(C5−H8)	1241	β(C5−H8)
1237vw	1236w														
1202s	1202w	1198	νN13-C14	1202	νN13-C14	1199	νN13-C14	1200	νN13-C14	1201	νN13-C14	1200	νN13-C14	1200	νN13-C14
	1142m	1145	β(C15−H18)	1138	β(C15−H18)	1145	β(C15−H18)	1144	β(C6−H9)	1141	β(C15−H18)	1140	β(C15−H18)	1145	β(C15−H18)
	1142m	1144	β(C6−H9)	1134	β(C6−H9)	1138	β(C6−H9)	1133	β(C15−H18)	1133	β(C6−H9)			1134	β(C6−H9)
1129s												1128	β(C6−H9)		
1097vw	1100m	1117	νC4-C5	1117	νC4-C5	1117	νC4-C5	1117	νC4-C5	1119	νC4-C5	1119	νC4-C5	1119	νC4-C5
			νC5-C6		νC5-C6		νC5-C6		νC5-C6						
1097vw	1100m	1110	νC17-C21	1112	νC17-C21	1110	νC17-C21	1112	νC17-C21	1112	β(C16−H20)	1112	β(C16−H20)	1112	νC21-C19
	1070vw	1101	νC1-N12	1103	νC1-N12	1104	νC1-N12	1099	νC1-N12	1093	νC1-N12	1095	νC1-N12	1095	νC1-N12
1027s	1026m	1032	βR_1 (A1)	1032	βR_1 (A1)	1032	βR_1 (A1)	1031	βR_1 (A1)	1027	βR_1 (A1)	1027	βR_1 (A1)	1027	βR_1 (A1)
1027s	1026m	1022	βR_1 (A2)	1023	βR_1 (A2)	1022	βR_1 (A2)	1022	βR_1 (A2)	1019	βR_1 (A2)	1019	βR_1 (A2)	1019	βR_1 (A2)
964vvw	978vw			957	γC15-H18			957	γC15-H18	968	γC6-H9	969	γC6-H9	968	γC6-H9
954vvw	956vw	954	γC6-H9	955	γC6-H9	954	γC6-H9	954	γC6-H9	959	γC15-H18	960	γC15-H18	963	γC15-H18
952vvw		947	β(N12−O25)	950	β(N12−O25)	946	β(N12−O25)	951	β (N12−O25)						
937w	938vw	944	γC15-H18			942	γC17-H22			935	β(N12−O25)	935	β(N12−O25)	934	β(N12−O25)
	911vw									917	γC2-H7	914	γC2-H7	917	γC2-H7
895m	896vw	896	γC2-H7	893	γC2-H7	896	γC2-H7	895	γC2-H7	899	γC16-H20	902	γC16-H20	899	γC16-H20
879m	886sh vw	889	γC16-H20	872	γC16-H20	889	γC16-H20	874	γC16-H20	890	νC14-C15	884	νC14-C15	884	νC14-C15
831m		829	γC5-H8	835	γC17-H22	832	γC5-H8	836	γC17-H22	832	γC5-H8	837	γC5-H8	832	γC5-H8
831m				831	γC5-H8			827	γC5-H8	829	γC17-H22	830	γC17-H22	829	γC17-H22
823s		822	γC17-H22	823	βR_2 (A1)	823	βR_2 (A1)	822	βR_2 (A1)						
819w	807vw	817	βR_2 (A1)			818	γC15-H18								
795w	795vw													797	ν C3−Cl10
782sh		771	νC19-Cl23			770	νC19-Cl23			786	ν C3−Cl10	788	ν C3−Cl10		
757vw				764	βR_2 (A2)			765	βR_2 (A2)						
718vw		724	τONNC	718	τONNC	716	τONNC	724	τONNC	712	τONNC	713	τONNC	712	τONNC
706m	706w									701	βR_3 (A2)	704	βR_3 (A2)		
694m	696w	687	τR_1 (A2)	696	τR_1 (A2)	696	τR_1 (A2)	690	τR_1 (A1)					685	βR_3 (A2)
683sh		681	τR_1 (A1)	680	βR_3 (A2)	681	βR_3 (A2)	683	τR_1 (A2)	686	τR_1 (A2)	687	τR_1 (A2)	683	τR_1 (A2)
678w	678m	680	βR_3 (A2)	677	τR_1 (A1)	677	τR_1 (A1)	677	βR_3 (A2)	679	βR_3 (A1)	678	βR_3 (A1)	676	βR_3 (A1)
673vw										672	τR_1 (A1)	672	τR_1 (A1)	670	τR_1 (A1)
663vw	661vw	662	βR_3 (A1)	666	βR_3 (A1)	665	βR_3 (A1)	662	βR_3 (A1)	658	βR_3 (A2)	656	βR_2 (A2)	666	βR_2 (A2)
637vw		641	γC19-Cl23	636	γC19-Cl23	638	γC19-Cl23	641	γC19-Cl23						

(*continued on next page*)

Table 2 (*continued*)

Experimental[a]		*Cis I*[a]		*Cis II*[a]		*Cis III*[a]		*Cis IV*[a]		*Trans I*[a]		*Trans II*[a]		*Trans III*[a]	
IR Solid	Raman	SQM[b]	Assig.[a]	SQM[b]	Assig.[a]	SQM[b]	Assig.[a]	SQM[b]	Assig.[a]	SQM[b]	Assig.[a]	SQM[b]	Assig.[a]	SQM[b]	Assig.[a]
604vw				598	τR_2 (A1)	596	τR_2 (A1)	594	γ(N12−C1)	595	γ(N13−C14)	594	γ(N13−C14)		
589vw		591	τR_2 (A1)											590	γ(N13−C14)
580w	580w			576	γ(N13−C14)			577	γ(N13−C14)			575	νC4-Cl11		
570sh		571	γ(N13−C14)												
556vw	557w					568	γ(N13−C14)			541	νC4-Cl11			544	νC4-Cl11
540vw	540vw	537	νC21-Cl24			538	νC21-Cl24			535	γ(N12−C1)			537	γ(N12−C1)
532vvw										533	νC21-Cl24	534	γ(N12−C1)		
528vw	527sh			526	νC4-Cl11 νC21-Cl24			528	νC4-Cl11 νC21-Cl24					529	νC21-Cl24
511vvw	514w			510	τR_2 (A1) γ (N12−C1)	511	ν C4−Cl11								
502vw		507	νC4-Cl11					508	τR_2 (A1)			507	νC21-Cl24		
492vw	492vw													478	β(C14−N13)
475vw	486vw														
469vw	470sh vw	466	β(C19−Cl23)			464	β(C21−Cl24)			460	νC19-Cl23	463	νC19-Cl23		
462w	461w			459	β(C19−Cl23)			461	β(C21−Cl24)	459	β(C3−Cl10)	459	β(C3−Cl10)	460	β(C19−Cl23)
440w	448vw	447	τR_3 (A1)	445	νC3-Cl10	450	νC3-Cl10	447	νC3-Cl10	441	τR_3 (A2)	442	τR_3 (A2)	443	τR_3 (A2)
	435vw	446	νC3-Cl10	439	τR_3 (A2)	438	τR_3 (A2)	440	τR_3 (A2)	440	τR_3 (A1)	437	τR_3 (A1)	441	νC19-Cl23
430w		435	τR_3 (A2)	435	τR_3 (A1)	435	τR_3 (A1)	437	τR_3 (A1)					439	τR_3 (A1)
422sh	422vw	429	γC4-Cl11			424	ν C19−Cl23 τR_2 (A1)			422	νC3-Cl10 βR_3(A1)				
415vw	408vw			408	νC19-Cl23			409	νC19-Cl23	405	β(C14−N13)	406	β(C14−N13)		
406vw															
396vw	391vw							397	τ CNNC βR_3 (A2)			387	β(C1−N12)		
	372vw	373	γC21-Cl24	379	βR_2 (A2) βR_3 (A2)	363	γC21-Cl24							367	νC21-Cl24 βR_2 (A2)
	361vw			358	β(C3−Cl10)	358	γ C21−Cl24 τ CNNC			365	γC21-Cl24	365	γC21-Cl24	363	γ C21−Cl24
	347vw	342	β(C3−Cl10)					343	βR_2 (A1) β (C3−Cl10)			355	βR_2 (A1)		
	337vw			334	γC21-Cl24			334	γC21-Cl24	336	βR_2 (A1)			340	βR_2 (A1)
		321	βR_2 (A2)			321	βR_2 (A2)								
	295w	286	βR_2 (A1) ν C1−N12	285	βR_2 (A2) βR_3 (A2)	286	βR_2 (A1) ν C1−N12	285	βR_2 (A2) βR_2 (A1)	292	γC4-Cl11	296	γC4-Cl11	291	γC4-Cl11
		279	γ(N12−C1)	279	γC4-Cl11	278	γC4-Cl11	280	γC4-Cl11	286	δ(C14−N13)	287	δ(C14−N13)	281	δ(C14−N13)
	223w	245	β(C14−N13)	249	δ(N12−C1)	247	β(C14−N13)	247	δ(N12−C1)	213	β(C4−Cl11)	218	βR_2 (A1) βR_2 (A2)	214	γC19-Cl23
	207w			208	γC3-Cl10					208	γC19-Cl23	208	γC19-Cl23	211	β(C4−Cl11)
		202	β(C4−Cl11)	200	β(C4−Cl11)	201	β (C3−Cl10)	204	β(C4−Cl11)	201	β(C21−Cl24)	200	β(C4−Cl11)	198	β(C21−Cl24)
		197	β (C21−Cl24)	197	β(C21−Cl24)	200	β(C4−Cl11)	198	β(C19−Cl23)			199	β(C21−Cl24)		
		181	τR_3 (A2) γ C19−Cl23			190	β(C19−Cl23)	190	β(C3−Cl10)	179	β(C1−N12)			173	β(C1−N12)
		168	γC3-Cl10	164	γ(N12−C1)	171	γC3-Cl10	167	γC3-Cl10	170	γC3-Cl10	167	γC3-Cl10	172	γC3-Cl10
		156	β(C1−N12)	151	β(C1−N12)	155	β(C1−N12)	158	β(C1−N12)	146	β(C19−Cl23)			159	β(C3−Cl10)
										138	τR_2 (A2)	135	τR_2 (A2)		
		132	τR_2 (A2)									131	β(C19−Cl23)	128	τR_2 (A2)
				115	τR_2 (A2)	119	τR_2 (A2)	120	τR_2 (A2)						
		90	τCC(A1)NN	84	τCC(A2)NN	90	τCC(A2)NN	87	τCC(A2)NN	86	τR_2 (A1)	90	τR_2 (A1)	84	τR_2 (A1)
		77		77	τ CNNC τ CC(A1)NN	78	τCNNC	77	τ CNNC τR_2 (A1)						
										58	δ(N12−C1)	57	δ(N12−C1)	57	δ(N12−C1)
										53	τCC(A2)NN	51	τCC(A2)NN	55	τCC(A2)NN
		32	τCNNC	26	τCC(A1)NN	30	γ(N12−C1)	32	τCNNC						
		24	τCC(A2)NN	25	τCNNC	26	τCC(A1)NN	24	β(C14−N13)	24	τCNNC	25	τCNNC	25	τCNNC
		20	δ(C14−N13)	22	β(C14−N13)	20	δ(C14−N13)	22	τCC(A1)NN δ(C14−N13)	16	τCC(A1)NN	16	τCC(A1)NN	14	τCC(A1)NN

Abbreviations: ν, stretching; β, deformation in the plane; γ, deformation out of plane; τ, torsion; β_R, deformation ring τ_R, torsion ring; ρ, rocking; δ, deformation; A1, Ring 1 (benzyl 1); A2, Ring 2 (benzyl 2).

[a] This work.

[b] From scaled quantum mechanics force field at B3LYP/6-31G*.

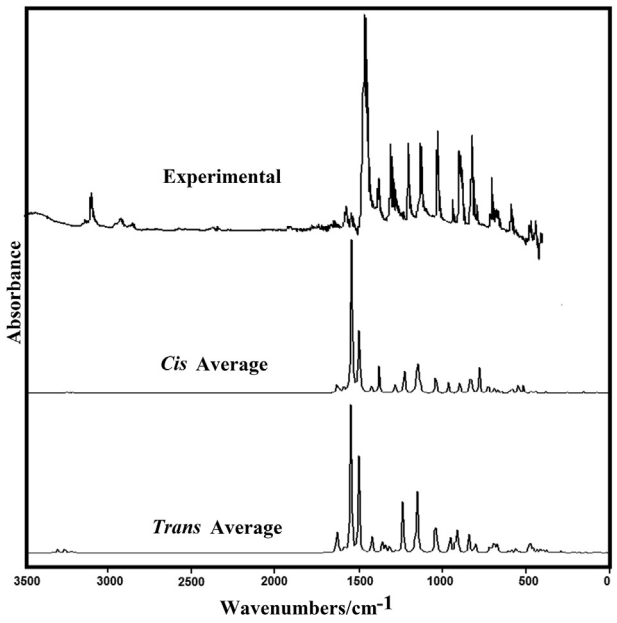

Fig. 3. Experimental infrared spectrum of TCAOB in the solid phase compared with the corresponding average predicted for all *Cis* and *Trans* isomers by using the B3LYP/6-31G* level of theory.

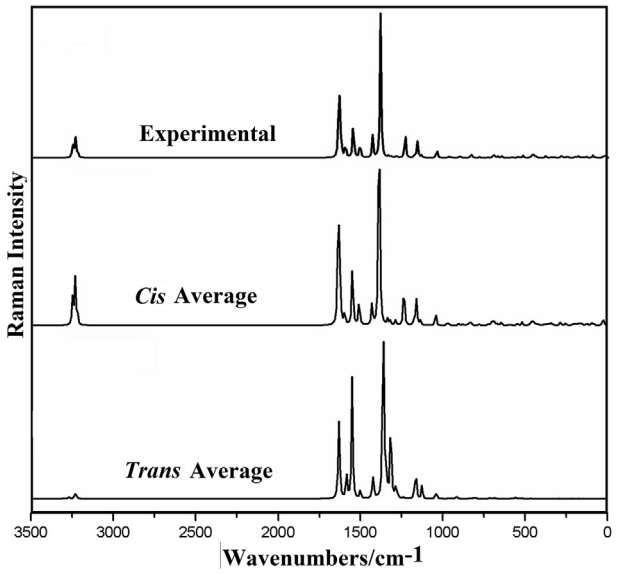

Fig. 4. Experimental Raman spectrum of TCAOB in the solid phase compared with the corresponding average predicted for all *Cis* and *Trans* isomers by using the B3LYP/6-31G* level of theory.

azoxybenzene derivatives, for all TCAOB isomers we have calculated the gap values and some interesting descriptors in order to know their reactivities and behaviours with both basis sets. Thus, the frontier orbitals and the chemical potential (μ), electronegativity (χ), global hardness (η), global softness (S), global electrophilicity index (ω) and global nucleophilicity index (E) descriptors were computed using both basis sets [37–40]. The gap values were calculated with the differences between the HOMO-LUMO values where the most reactive isomer present a low gap value while the equations used to calculate those descriptors were presented as support material in Table S14 because they are widely known. Here, the presences of lone pairs on the O and N atoms and of four

Table 3
Comparison of scaled internal force constants for all TCAOB isomers.

B3LYP method							
Force constant	*Cis I*	*Cis II*	*Cis III*	*Cis IV*	*Trans I*	*Trans II*	*Trans III*
TCAOB/6-31G*[a]							
f(C–N)	4.385	4.387	4.384	4.391	4.975	4.974	4.961
f(N=N)	8.273	8.272	8.279	8.264	8.316	8.332	8.326
f(N=O)	8.973	8.972	8.960	8.977	8.245	8.248	8.244
f(C–Cl)	3.477	3.475	3.481	3.474	3.460	3.454	3.466
$f(C-C)_{ring}$	6.473	6.479	6.481	6.483	6.476	6.476	6.471
f(C–H)	5.274	5.275	5.267	5.274	5.343	5.344	5.345
TCAOB/6-311++G**[a]							
f(C–N)	4.246	4.250	4.247	4.253	4.828	4.825	4.807
f(N=N)	8.266	8.263	8.279	8.262	8.228	8.250	8.244
f(N=O)	8.514	8.504	8.496	8.510	7.797	7.802	7.785
f(C–Cl)	3.421	3.420	3.425	3.420	3.407	3.402	3.410
$f(C-C)_{ring}$	6.358	6.364	6.364	6.366	6.349	6.351	6.345
f(C–H)	5.185	5.188	5.183	5.184	5.248	5.248	5.250

Force constant	*Cis I*	*Cis II*	*Trans I*	*Trans II*
TCAB/6-31G*[b]				
f(C–N)	4.001	4.016	4.958	4.948
f(N=N)	10.296	10.293	9.583	9.583
$f(C-C)_{ring}$	6.436	6.444	6.447	6.446
f(C–Cl)	3.456	3.455	3.430	3.443
f(C–H)	5.253	5.254	5.261	5.273
TCAB/6-311++G**[b]				
f(C–N)	3.903	3.908	4.847	4.838
f(N=N)	10.195	10.191	9.558	9.558
$f(C-C)_{ring}$	6.320	6.329	6.325	6.324
f(C–Cl)	3.400	3.399	3.374	3.388
f(C–H)	5.169	5.169	5.186	5.188

Units are mdyn $Å^{-1}$ for stretching and stretching/stretching interaction.
[a] This work.
[b] From Ref [22].

electronegative Cl atoms produce attractive properties to TCAOB, as suggested by the above studies. The results clearly show that: (i) the both frontier orbitals are localized on the rings, as in TCAB [22], (ii) the *Trans* isomers are more reactive than the *Cis* ones because they present low gap values, (iii) the nucleophilicity are highest in the *Trans* forms than the *Cis* ones, (iv) the energies gap follows the trend: *Trans II* > *Cis II* > *Cis IV* > *Cis I* > *Cis III* > *Trans III* > *Trans I*, being the *Trans I* isomer the most reactive probably due to the repulsion of the more electronegative Cl and O atoms as a consequence of their proximities and, finally, (v) the TCAOB is kinetically more inert than TCAB because present a higher stability and high chemical hardness, evidently justified by the presence of N=O bond in TCAOB.

4.8. Electronic spectrum

The electronic spectrum of TCAOB registered in an ethanol solution compared with the corresponding predicted for all isomers in the same medium at the B3LYP/6-31G* level of theory can be seen in Fig. 5 while Fig. S9 shows the comparisons between the experimental electronic spectra of TCAB and TCAOB in ethanol solution. In both spectra it is possible to observe a very strong band located at 335 nm in TCAB (molar absortivity = 1600 $M^{-1}cm^{-1}$) while at 337 nm in TCAOB (molar absortivity = 1700 $M^{-1}cm^{-1}$) that can be easily assigned to $\pi \rightarrow \pi^*$ and $n \rightarrow \pi^*$ transitions because under UV–vis radiation (>200 nm) the presence of π-electrons and lone-pairs electrons (n-electrons) permit the electronic transitions of these types [23,45]. Besides, in the UV–visible spectrum of TCAB there is a very weak band at 445 nm no observed in TCAOB while the weak band at 271 nm is only observed in TCAOB. Hence, this latter band should evidently be assigned to $n \rightarrow \pi^*$ transitions due to N=O chromophore. On the other hand, the UV–vis spectra

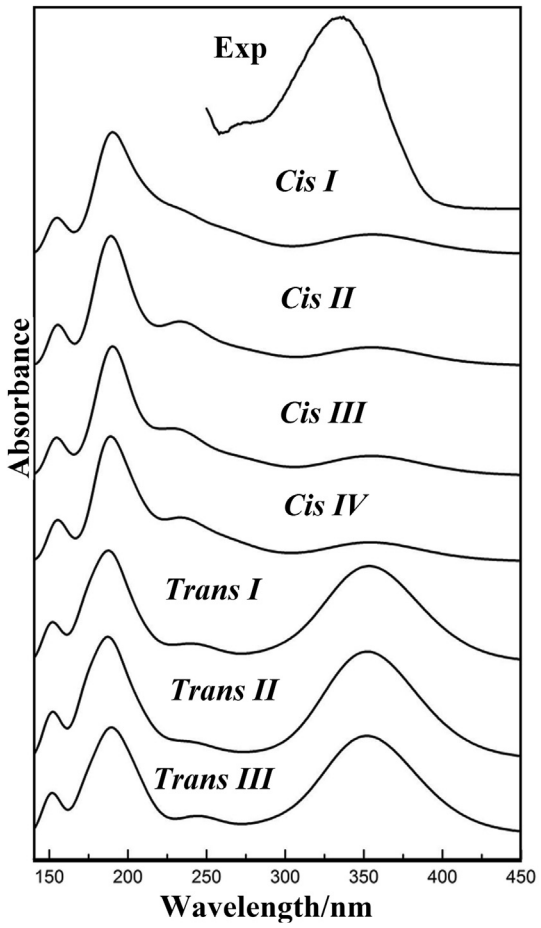

Fig. 5. Experimental electronic spectrum of TCAOB in ethanol solution compared with the corresponding predicted for all *Cis* and *Trans* isomers by using the B3LYP/6-31G* level of theory.

predict four bands for all TCAOB isomers, showing the *Cis* isomers bands with low intensities, as observed in Fig. 5. In these spectra we observed a bathochromic shift toward longer wavelengths probably due to the conjugation among the lone pairs of O25 atoms and the four Cl atoms present in TCAOB. The predicted positions of the four UV–vis bands in the *Trans* isomers are: 353/355 nm; 249 nm, 189 nm and 151/155 nm while for the Cis forms, these bands are located at 358 nm, 234 nm, 187/196 nm and 154/159 nm. Obviously, all these bands observed are attributed to the $\pi \rightarrow \pi^*$ and $n \rightarrow \pi^*$ transitions due to the C=C, N=N and N=O chromophores groups, where the most intense can be assigned to $\pi \rightarrow \pi^*$ transitions of C=C groups. Note that the predicted bands observed at low wavelengths were not observed in the experimental spectra because this was recorded from 220 to 600 nm.

5. Conclusions

The toxic TCAOB derivative was synthesized and, then, characterized it in the solid state by infrared and Raman spectroscopies and, in solution by multidimensional nuclear magnetic resonance (NMR) and ultraviolet–visible spectroscopies. The molecular structures of four *Cis* isomers and three *Trans* isomers were determined in gas phase by using the B3LYP method and the 6-31G* and 6-311++G** basis sets. NBO studies support the high stability of both *Cis* and *Trans* isomers due to their $\pi \rightarrow \pi^*$, $n \rightarrow \sigma^*$, $n \rightarrow \pi^*$ and $\pi^* \rightarrow \pi^*$ electronic transitions while the AIM studies suggest the existence of intra-molecular C–H···O hydrogen bonds in the *Trans* forms, as revealed by the broad IR band in the higher wavenumbers region. The *Trans I* isomer presents the higher reactivity, as suggested by their low gap energy probably due to the repulsion of the more electronegative Cl and O atoms as a consequence of their proximities. Here, the complete assignments of the 69 normal modes of vibration for all TCAOB isomers were reported by using the SQMFF methodology. The presence of the N=O group in TCAOB support the increase in the intensity of the IR band centred in 3440 cm^{-1}, the shifting of the bands assigned to the CH stretching modes, the notable increase in the intensities of bands observed between 1800/1500 and 1400/600 cm^{-1} and the decrease in the intensities of bands between 1300 and 900 cm^{-1}, as compared with the corresponding spectrum of TCAB. In addition, the lower $f(N{=}N)$ and $f(C{-}C)_{ring}$ force constants values for the *Trans* forms of TCAOB could be probably related to the strong $\pi \rightarrow \pi$ delocalizations observed by NBO analysis due to the planarity of those two forms, as also was observed in the *Trans* forms of TCAB.

Acknowledgements

This work was supported with grants from CIUNT Project Nº 26/D507 (Consejo de Investigaciones, Universidad Nacional de Tucumán) and CONICET (Consejo Nacional de Investigaciones Científicas y Técnicas, R. Argentina). The authors thank to Dr. V. Daier (IQUIR) for the UV–Visible spectrum and to Prof. T. Sundius for the Molvib program.

Appendix A. Supplementary data

Supplementary data related to this article can be found at http://dx.doi.org/10.1016/j.molstruc.2017.04.043.

References

[1] D.D. Kaufman, J.R. Plimmer, J. Iwan, U.I. Klingebiel, 3,3',4,4'-Tetrachloroazoxybenzene from 3,4-dichloroaniline in microbial culture, J. Agric. Food Chem. 20 (4) (1972) 916–919.
[2] R. Bartha, D. Pramer, Pesticide transformation to aniline and azo compounds in soil, Science 156 (1967) 1617–1618.
[3] B.P. Singh, A. Nyska, G.E. Kissling, W. Lieuallen, S.L. Johansson, D.E. Malarkey, M.J. Hooth, Urethral carcinoma and hyperplasia in male and female B6C3F1 mice treated with 3,30,4,40-tetrachloroazobenzene (TCAB), Toxicol. Pathol. 38 (2010) 372–381.
[4] J. Hooth, Urethral carcinoma and hyperplasia in male and female B6C3F1 mice treated with 3,3',4,4'-tetrachloroazobenzene (TCAB), Toxicol. Pathol. 38 (2010) 372–381.
[5] I.J. Badovinac, N. Orlić, C. Gellini, L. Moroni, P.R. Salvi, Micro-Raman and computational study of the azoxybenzene photorearrangement to 2-hydroxyazobenzene, J. Mol. Struct. 924–926 (2009) 62–65.
[6] N.J. Bunce, Jean-Pierre Schoch, Michael C. Zerner, Photorearrangement of azoxybenzene to 2-hydroxyazobenzene. Evidence for electrophilic substitution by oxygen, J. Am. Chem. Soc. 99 (24) (1977) 7986–7991.
[7] V. Cantatore, G. Granucci, M. Persico, Simulation of the $\pi \rightarrow \pi^*$ photodynamics of azobenzene: decoherence and solvent effects, Comp. Theor. Chem. 1040 (2015) 126–135.
[8] P. Cattaneo, M. Persico, An *ab initio* study of the photochemistry of azobenzene, Phys. Chem. Chem. Phys. 1 (20) (1999) 4739–4743.
[9] G. Chilaya, A. Chanishvili, G. Petriashvili, R. Barberi, M.P. de Santo, M.A. Matranga, Different approaches of employing cholesteric liquid crystals in dye lasers, Mater. Sci. Appl. 2 (2011) 116–129.
[10] R. Cimiraglia, M. Persico, J. Tomasi, Azoxy compounds and oxadiaziridines. An ab initio study of the ring closure reactions and of the Cis-Trans isomerizations, J. Phys. Chem. 81 (19) (1977) 1876–1882.
[11] Ai-Hua Gao, Bin Li, Pei-Yu Zhang, Jianyong Liu, Photochemical Dynamics Simulations for trans–cis Photoisomerizations of Azobenzene and Bridged Azobenzene 1031, 2014, pp. 1–82.
[12] S.-B. Rhee, H.H. Jaffé, Photochemical and thermochemical cis-trans isomerization of azoxybenzene, J. Am. Chem. Soc. 95 (17) (1973) 5518–5521.
[13] S.V. Serak, N.V. Tabiryan, G. Chilaya, A. Chanishvili, G. Petriashvili, Chiral azobenzene nematics Phototunable with a green laser beam, Mol. Cryst. Liq. Cryst. 488 (2008) 42–55.
[14] J. Shao, Y. Lei, Z. Wen, Y. Dou, Z. Wang, Non-adiabatic simulation study of photoisomerization of azobenzene: detailed mechanism and load-resisting

capacity, J. Chem. Phys. 129 (16) (2008) 164111.
[15] E.M.M. Tan, S. Amirjalayer, S. Smolarek, A. Vdovin, F. Zerbetto, W.J. Buma, Fast photodynamics of azobenzene probed by scanning excited-state potential energy surfaces using slow spectroscopy, Nat. Commun. 6 (2015) 5860.
[16] A. Cembran, F. Bernardi, M. Garavelli, L. Gagliardi, G. Orlando, On the mechanism of the cis-trans isomerization in the lowest electronic states of azobenzene: S_0, S_1, and T_1, J. Am. Chem. Soc. 126 (2004) 3234–3243.
[17] D. Aronzon, E.P. Levy, P.J. Collings, A. Chanishvili, G. Chilaya, G. Petriashvili, Trans-cis isomerization of an azoxybenzene liquid crystal, Liq. Cryst. 34 (6) (2007) 707–718.
[18] T. Tsuji, H. Takashima, H. Takeuchi, T. Egawa, S. Konaka, Molecular structure of trans-azoxybenzene determined by gas electron diffraction combined with ab initio calculations, J. Mol. Struct. 554 (2000) 203–210.
[19] K. Ejsmont, A.A. Domanski, J.B. Kyziol, J. Zaleski, Trans-4-Bromo-ONN-azoxybenzene at 100 K, Acta Cryst. C 60 (Pt 5) (2004) o368–o370.
[20] S.P. González Martínez, S. Bernès, *trans*-Diphenyldiazene oxide, Acta Cryst. E63 (2007) o3639.
[21] S.J. Kavitha, S. Chandrasekar, K. Panchanatheswaran, Trans-1,2-Bis(3-chlorophenyl)diazene oxide, Acta Cryst. E59 (2003) o947–o949.
[22] M.V. Castillo, J.L. Pergomet, G.A. Carnavale, L. Davies, J. Zinczuk, S.A. Brandán, A complete vibrational study on a potential environmental toxicant agent, the 3,3,4,4-tetrachloroazobenzene combining the FTIR, FTRaman, UV–Visible and NMR spectroscopies with DFT calculations, Spectrochim. Acta A 134 (2015) 577–586.
[23] C. Cojocaru, A. Airinei, N. Fifere, Molecular Structure and Modeling Studies of Azobenzene Derivatives Containing Maleimide Groups vol. 2, SpringerPlus, 2013, p. 586.
[24] A.E. Reed, L.A. Curtis, F. Weinhold, Intermolecular interactions from a natural bond orbital, donor-acceptor viewpoint, Chem. Rev. 88 (6) (1988) 899–926.
[25] E.D. Glendening, J.K. Badenhoop, A.D. Reed, J.E. Carpenter, F. Weinhold, NBO 3.1; Theoretical Chemistry Institute, University of Wisconsin, Madison, WI, 1996.
[26] R.F.W. Bader, Atoms in Molecules, a Quantum Theory, Oxford University Press, Oxford, 1990. ISBN: 0198558651.
[27] F. Biegler-Köning, J. Schönbohm, D. Bayles, AIM2000; a program to analyze and visualize atoms in molecules, J. Comput. Chem. 22 (2001) 545–559.
[28] A.D. Becke, Density functional thermochemistry. III. The role of exact exchange, J. Chem. Phys. 98 (1993) 5648–5652.
[29] C. Lee, W. Yang, R.G. Parr, Development of the Colle-Salvetti correlation-energy formula into a functional of the electron density, Phys. Rev. B 37 (1988) 785–789.
[30] E. Gagnon, B.T. Newbold, Peracetic acid oxidation of halogenated azobenzenes, Can. J. Chem. 37 (1959) 366.
[31] A.B. Nielsen, A.J. Holder, Gauss View 5.0, User's Reference, Gaussian Inc., Pittsburgh, PA, 2009.
[32] M.J. Frisch, G.W. Trucks, H.B. Schlegel, G.E. Scuseria, M.A. Robb, J.R. Cheeseman, G. Scalmani, V. Barone, B. Mennucci, G.A. Petersson, H. Nakatsuji, M. Caricato, X. Li, H.P. Hratchian, A.F. Izmaylov, J. Bloino, G. Zheng, J.L. Sonnenberg, M. Hada, M. Ehara, K. Toyota, R. Fukuda, J. Hasegawa, M. Ishida, T. Nakajima, Y. Honda, O. Kitao, H. Nakai, T. Vreven, J.A. Montgomery Jr., J.E. Peralta, F. Ogliaro, M. Bearpark, J.J. Heyd, E. Brothers, K.N. Kudin, V.N. Staroverov, R. Kobayashi, J. Normand, K. Raghavachari, A. Rendell, J.C. Burant, S.S. Iyengar, J. Tomasi, M. Cossi, N. Rega, J.M. Millam, M. Klene, J.E. Knox, J.B. Cross, V. Bakken, C. Adamo, J. Jaramillo, R. Gomperts, R.E. Stratmann, O. Yazyev, A.J. Austin, R. Cammi, C. Pomelli, J.W. Ochterski, R.L. Martin, K. Morokuma, V.G. Zakrzewski, G.A. Voth, P. Salvador, J.J. Dannenberg, S. Dapprich, A.D. Daniels, Ö. Farkas, J.B. Foresman, J.V. Ortiz, J. Cioslowski, D.J. Fox, Gaussian 09, Revision D.01, Gaussian Inc, Wallingford CT, 2009.
[33] B.H. Besler, K.M. Merz Jr., P.A. Kollman, Atomic charges derived from semi-empirical methods, J. Comp. Chem. 11 (1990) 431–439.
[34] a) G. Rauhut, P. Pulay, Transferable scaling factors for density functional derived vibrational force fields, J. Phys. Chem. 99 (1995) 3093–3100;
b) G. Rauhut, P. Pulay, J. Phys. Chem. 99 (1995) 14572.
[35] T. Sundius, Molvib-a flexible program for force field calculations, J. Mol. Struct. 218 (1990) 321–326.
[36] R. Ditchfield, Self-consistent perturbation theory of diamagnetism. I. A gage-invariant LCAO (linear combination of atomic orbitals) method for NMR chemical shifts, Mol. Phys. 27 (1974) 789–807.
[37] R.G. Parr, R.G. Pearson, Absolute hardness: companion parameter to absolute electronegativity, J. Am. Chem. Soc. 105 (1983) 7512–7516.
[38] D. Romani, S.A. Brandán, M.J. Márquez, M.B. Márquez, Structural, topological and vibrational properties of an isothiazole derivatives series with antiviral activities, J. Mol. Struct. 1100 (2015) 279–289.
[39] M.B. Márquez, S.A. Brandán, A structural and vibrational investigation on the antiviral deoxyribonucleoside thymidine agent in gas and aqueous solution phases. 0020-7608, Int. J. Quantum Chem. 114 (3) (2014) 209–221.
[40] D. Romani, S. Tsuchiya, M. Yotsu-Yamashita, S.A. Brandán, Spectroscopic and structural investigation on intermediates species structurally associated to the tricyclic bisguanidine compound and to the toxic agent, saxitoxin, J. Mol. Struct. 1119 (2016) 25e38.
[41] P.C. Chen, Y.C. Chieh, Azobenzene and stilbene: a computational study, J. Mol. Struct. (Theochem) 624 (2003) 191–200.
[42] A. Mostad, C.H.R. Rømming, A refinement of the crystal structure of cis-azobenzene, Acta Chem. Scand. 25 (1971) 3561–3568.
[43] M. Dubecký, R. Derian, L. Mitas, I. Štich1, Ground and excited electronic states of azobenzene: a quantum Monte Carlo study, J. Chem. Phys. 133 (2010) 244301–244305.
[44] M.G.R. Priya, T. Srinivasan, K. Girija, N. RaviChandran, D. Velmurugan, 3-(4-Chlorophenyl)quinazolin-4(3H)-one, Acta Cryst. E67 (2011) o2310.
[45] Y. Ye, J. Pang, X. Zhou, J. Huang, Understanding the torsion effects on optical properties of azobenzene derivatives, Comp. Theor. Chem. 1076 (2016) 17–22.